Nanoscale observations of leaching of sensitive clay

Dorsa Saaedifar[1*], *Angela* Casarella[2], *Stephen* Hall[3], and *Jelke* Dijkstra[1]

[1] Department of Architecture and Civil Engineering, Chalmers University of Technology, Gothenburg, Sweden
[2] Department of Civil and Environmental Engineering, Imperial College London, London, United Kingdom
[3] Division of Solid Mechanics, Lund University, Lund, Sweden

1 Introduction

Sensitive clays are fine-grained geomaterials that experience substantial strength loss when disturbed. This behaviour is measured by the sensitivity S_t, defined as the ratio of intact peak strength to remoulded undrained shear strength. According to Swedish criteria, clay is classified as quick if $S_t \geq 50$ and the fully remoulded undrained shear strength is below 0.4 kPa [1]. Such clays can collapse rapidly from a solid-like to a fluid-like state under hydro-mechanical disturbance [2]. Owing to this abrupt strength loss, sensitive or quick clay deposits pose a major landslide hazard, as documented by events such as Surte (1952), Tuve (1977), and Levanger (2025).

Sensitive marine clays are typically composed of clay mineral assemblages dominated by illite and chlorite, with additional contributions from kaolinite, smectite, and mixed-layer illite-smectite (I/S) phases [3, 4]. After deposition, these assemblages may continue to evolve through pore water changes. For example, smectite can progressively transform towards illite through mixed-layer I/S phases when K^+ is available from feldspar or mica dissolution [5]. Furthermore, post-depositional leaching is widely regarded as a key process in the evolution of sensitive marine clays. Early work linked quick-clay behaviour to progressive salt removal from pore water after deposition [6, 7], and subsequent studies showed that sensitivity is strongly controlled by pore water chemistry [8, 9].

Despite this established geotechnical and geochemical framework, the nanoscale structural response to leaching is not well understood. In particular, the direct structural link between salt removal and changes in bonding remains unclear. To address this gap, a non-destructive method is required that can characterise clay in its saturated consolidated state without altering its structure. Wide-angle X-ray scattering (WAXS) is well suited to this purpose, as it can non-destructively capture small-scale mineralogical features, sub-particle clay behaviour, and basal-level structural changes ensuring continuous saturation of the tested samples. X-ray scattering techniques have been used to study hydration transitions, swelling-related basal-spacing changes, and nanoscale response in clays [10, 11] and WAXS has shown to resolve mineralogical features and unit-layer scale structural distances in saturated clay [12, 13]. The novelty of this study lies in applying WAXS to identify unit-layer structural changes induced by salt leaching. Accordingly, this study investigates the unit-layer structural changes caused by pore water salt removal in natural sensitive Kärra clay, by comparing natural and leached states using WAXS at the MAX IV synchrotron facility. The latter enables fast measurements of changes in structure spanning from Å to nm.

2 WAXS theoretical background

WAXS is based on elastic X-ray scattering from variations in electron density and provides structural information at the nanoscale. For monochromatic radiation, constructive interference follows Bragg's law (Equation (1)), where λ is the X-ray wavelength, d is some characteristic spacing in the material, and θ is the scattering angle,

$$n\lambda = 2d\sin\theta. \tag{1}$$

In reciprocal-space analysis, the scattering vector q is used (Equation (2)) and the characteristic spacing d is obtained from the scattering angle corresponding to characteristic peaks in the WAXS signal, following Equation (3),

$$q = \frac{4\pi}{\lambda}\sin\theta, \tag{2}$$

$$d = \frac{2\pi}{q}. \tag{3}$$

Peak position, defined by is the scattering angle, θ, reflects characteristic spacing, d, whereas peak width and intensity reflect structural coherence and order in the material under study. In addition to Bragg reflections, diffuse intensity beneath and between peaks reflects less ordered (or amorphous) structural contributions.

In X-ray scattering patterns, the shape and contrast of Bragg reflections are governed by structural order and coherent domain size, as illustrated in Figure 1. Peak broadening (Figure 1a), i.e., increased reflection width and reduced peak height, relates to smaller coherent domains and reduced stacking coherence in layered silicates. When the position of the peak shifts, there is a uniform strain. The degree of order also influences how rapidly peak intensities decay with increasing scattering vector q, where better-ordered structures retain observable reflections to higher q, while more disordered structures show faster intensity decay. Baseline (normalised) intensity level (Figure 1b) represents an increase

* Corresponding author: dorsa.saaedifar@chalmers.se

in diffuse background intensity beneath and between Bragg reflections, consistent with a larger contribution from poorly ordered or amorphous constituents that scatter broadly rather than producing sharp peaks [14]. In natural clay-rich soils, a narrow, high-intensity reflection on a low baseline, therefore, indicates relatively well-stacked, crystalline layer domains, whereas a broader reflection combined with a higher baseline indicates less coherent stacking and a larger proportion of structurally disordered or amorphous material contributing predominantly to diffuse background scattering rather than distinct Bragg reflections.

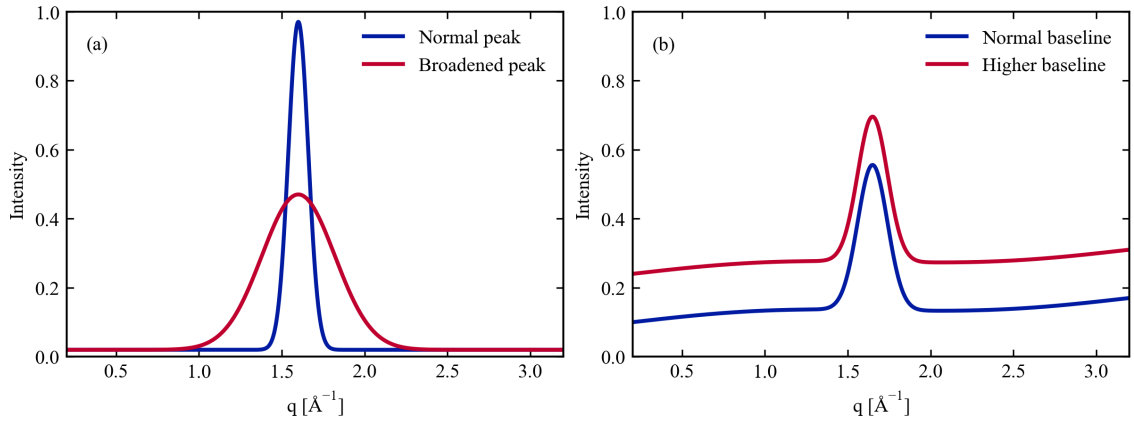

Figure 1. Schematic WAXS descriptors: (a) peak broadening at fixed *q*-position, (b) baseline movement.

3 Materials and methods

Natural sensitive clay used in this study was sampled at a depth of 8 m from the Chalmers soft soil test site near Kärra (Gothenburg, Sweden) using a STII piston sampler. According to the Swedish classification system, the clay at this depth exhibits a sensitivity greater than 6. Kärra clay had a natural water content of 70% with a pore water salinity of 0.468 M.

Two subsamples, with a diameter of 50 mm and a height of 20 mm, were prepared from the intact sample for salt leaching. This procedure was conducted in a Rowe cell by first saturating the specimens and then applying controlled leaching to achieve 10% and 24% salt removal. Before starting the leaching process, a B-check was conducted to make sure the sample was totally saturated. During leaching, the effective stress was maintained at the in-situ value to avoid loading effects. The water content increased from 70% in the natural state to 75% after leaching, confirming full saturation.

To characterise pore water chemistry, water content and major cation concentrations (Na^+, K^+, Mg^{2+}, Ca^{2+}) were determined for the natural and leached samples with ion chromatography. Cation concentrations were measured by a Dionex ICS-900 system (Thermo Fisher Scientific) equipped with a162 Dionex IonPac CS12A cation-exchange column and a suppressed conductivity detector on aqueous extracts obtained from the soil-water system after centrifugation and filtration. Water content and major-ion concentrations are reported in Table 1.

Table 1. Water content and major cations concentrations according to ion chromatography results.

Sample	Water content (%)	Na^+ (M)	K^+ (M)	Mg^{2+} (M)	Ca^{2+} (M)	Total cations (M)
Natural Kärra	70	0.422	0.021	0.014	0.011	0.468
Kärra with 10% salt removal	75	0.384	0.017	0.013	0.008	0.422
Kärra with 24% salt removal	75	0.322	0.015	0.011	0.007	0.355

For WAXS analysis, the subsamples were cored into quartz capillaries with 1 mm diameter and 10 µm wall thickness from the intact and leached samples. The capillaries were sealed at both ends to prevent moisture loss during measurement. The WAXS measurements were carried out at the CoSAXS beamline at MAX IV Synchrotron Facility (Lund, Sweden) using a monochromatic X-ray beam of 18 keV (λ = 0.68880 Å). X-ray scattering data were recorded with a Pilatus 2M detector with a pixel size 172 µm at a sample-to-detector distance of 0.4374 m. Empty capillary background and detector corrections were applied and all datasets were processed using the same background subtraction and intensity normalisation. To assess repeatability, a line scan was conducted for each subsample, by collecting measurements at multiple points along a vertical line spanning the sample height. resulting This resulted in 30 measurements for intact Kärra, 24 measurements for the 10% salt-removal sample, and 9 measurements for the 24% salt-removal sample. The WAXS measurements showed comparable responses, and one representative measurement reflecting the overall trend was selected for presentation.

4 Results and discussion

Figure 2 illustrates the extracted 1D WAXS profiles (based on radial integration of the 2D data) of natural Kärra (blue), Kärra with 10% salt removal (black), and Kärra with 24% salt removal (red). The most pronounced leaching effect occurs in the low q range (large features, $q < 0.6$ Å^{-1}, $d > 10.47$ Å), where both leached samples show elevated intensities relative to the natural state. Additional effects are observed at high q range. Given that identical correction procedures were applied to all datasets, this behaviour reflects no change in fabric in the sample but increased scattering intensity due to a higher density of the solids. This could be because of sample-to-sample variation in water content and mineralogical composition. The baseline response is already pronounced at 10% salt removal, whereas the 24% pattern remains close in baseline level, suggesting that most structural change occurs during early leaching stages and further leaching introduces only limited additional change. For example, at $q = 0.3$ Å^{-1} the intensity increased more than 3 times.

The principal Bragg peak positions remain unchanged within experimental resolution, indicating that the main crystalline spacings are preserved during leaching. Illite related reflections [3] remain at $q \approx 0.63$ Å^{-1} ($d = 10$ Å) with higher order illite contributions near $q \approx 1.26$ and 2.51 Å^{-1} in all samples. The leached patterns, particularly at 24% salt removal, show generally higher and sharper peak intensities. This is consistent with a leaching-induced fabric adjustment (particle rearrangement/partial consolidation during the leaching path), which can enhance coherent Bragg scattering without changing peak position.

A different behaviour is observed for the illite-smectite mixed-layer (I/S) at $q \approx 0.68$ Å^{-1} [15], which broadens at 10% salt removal and then shifts with leaching at 24% salt removal. This is consistent with reduced stacking regularity/coherence in mixed-layer illite-smectite domains [16]. Interlayer K^+ is a key stabilising cation in illitic layers, and previous studies show that I/S expandability depends on cation state and reaction history rather than on a single monotonic K trend [17, 18]. In this context, the observed broadening with leaching is interpreted as compatible with changes in interlayer conditions during leaching (including reduced available K^+), which may alter stacking regularity and mixed-layer organisation. However, WAXS alone cannot uniquely separate electrochemical effects from mechanical fabric changes.

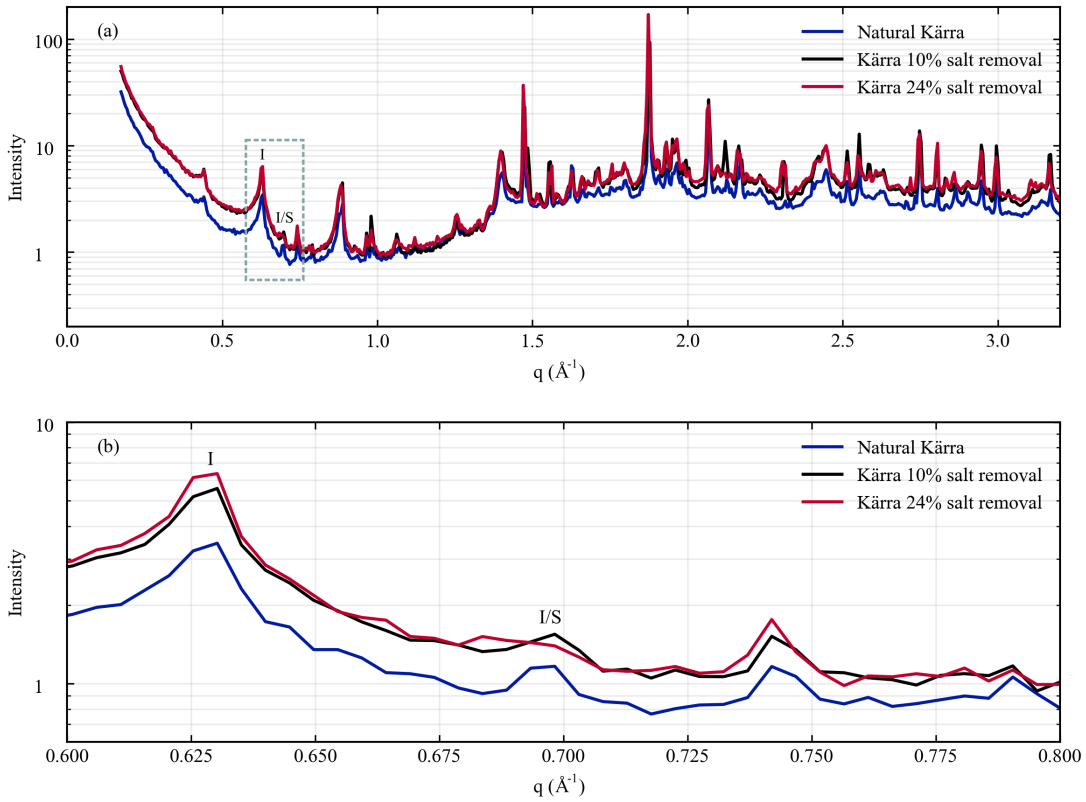

Figure 2. WAXS intensity profiles of natural Kärra clay (blue), Kärra with 10% salt removal (black), and Kärra with 24% salt removal (red): (a) Full I(q) pattern. (b) Enlarged view of the q = 0.60 to 0.80 Å^{-1} range, indicated by the dashed box in section (a).

5 Conclusion

WAXS measurements have been carried out on natural Kärra clay and leached Kärra clay samples (10% and 24% salt removal) to investigate leaching-related nanoscale structural evolution in a natural sensitive clay. This focus was motivated by the established role of salinity reduction in the development of sensitivity in marine clays.

The main effect of leaching was observed in the low q region, where both leached samples showed elevated baseline intensity relative to natural Kärra clay, indicating increased diffuse scattering. Since the low q increase was already

pronounced at 10% salt removal and changed only slightly at 24%, much of the structural evolution appears to occur during the early stage of leaching.

The principal Bragg peak positions remained essentially unchanged, indicating preservation of the main crystalline spacings. Illite related reflections remained present in all samples, while the I/S peak near $q \approx 0.68$ Å^{-1} broadened progressively, with the most significant broadening at 24% leaching, indicating reduced stacking coherence in the mixed-layer fraction. This evolution may reflect a combination of fabric rearrangement during leaching and electrochemical re-equilibration during desalination, including possible effects of reduced K^+ on interlayer or interparticle interactions.

Overall, leaching altered the balance between ordered and disordered structural domains, reflected in changes in diffuse background and Bragg reflection intensity, while the fundamental illite periodicities remained unchanged. These findings show that WAXS is well suited for detecting leaching-induced nanostructural and mineralogical modification as it enables the clay to be examined in its natural saturated state, hence, preserving the natural structure of the clay. However, WAXS alone cannot uniquely resolve the respective contributions of mechanical fabric rearrangement and electrochemical effects. The results presented here are limited to inter-layer structural evolution at the nanoscale and do not capture the evolution of the clay matrix fabric; therefore, any extrapolation to macroscopic behaviour remains premature and will be addressed in future work integrating nanometric, microscopic, and in situ testing approaches. A logical next step would be to perform integrated SAXS/WAXS to also cover the changes at aggregate level. Furthermore, by studying the changes across different sensitive clays and higher degrees of leaching more pronounced differences that are unique to quick clay can be isolated.

The financial support of Vetenskapsrådet under grants 2020-03982 & 2022-03809 is greatly acknowledged.

References

1. K. Rankka, Y. Andersson-sköld, C. Hultén, R. Larsson, V. Leroux, T. Dahlin, Quick clay in Sweden. Swedish Geotechnical Institute (SGI) (2004).
2. J. K. Torrance, Landslides in quick clay. Landslides: types, mechanisms and modeling, 83–94 (2012). https://doi.org/10.1017/CBO9780511740367.009
3. J. K. Mitchell, K. Soga, Fundamentals of soil behavior. John Wiley & Sons, Hoboken (2005).
4. R. Stevens, Glaciomarine fine sediments in southwestern Sweden: late Weichselian–Holocene lithography, depositional environments and varve formation. Ph.D. thesis, University of Göteborg, Department of Geology, Göteborg (1987).
5. H. Chamley, Clay mineralogy. Springer, Berlin (1989).
6. I. T. Rosenqvist, Om leirers kvikkagtighet. Technical Report Meddelande Nr. 4, Statens Vegvesen, Veglaboratoriet, Oslo (1946). In Norwegian.
7. I. T. Rosenqvist, Considerations on the sensitivity of norwegian quick-clays. Géotechnique **3**, 195–200 (1953). https://doi.org/10.1680/geot.1953.3.5.195
8. L. Bjerrum, I. T. Rosenqvist, Some experiments with artificially sedimented clays. Géotechnique **6**, 124–136 (1956). https://doi.org/10.1680/geot.1956.6.3.124
9. G. Meijer, J. Dijkstra, A novel methodology to regain sensitivity of quick clay in a geotechnical centrifuge. Can. Geotech. J. **50**, 995–1000 (2013). https://doi.org/10.1139/cgj-2012-0466
10. G. J. da Silva, J. O. Fossum, E. DiMasi, K. J. Måløy, Hydration transitions in a nanolayered synthetic silicate: A synchrotron x-ray scattering study. Phys. Rev. B **67**, 094114 (2003). https://doi.org/10.1103/PhysRevB.67.094114
11. G. Birmpilis, S. A. Hall, S. Lages, J. Dijkstra, Monitoring of the nano-structure response of natural clay under mechanical perturbation using small angle X-ray scattering and digital image correlation. Acta Geotech. **14**, 1965–1975 (2019). https://doi.org/10.1007/s11440-019-00832-8
12. A. Casarella, G. Birmpilis, J. Dijkstra, Experimental insight into the thermal nanometric response of clays. In Symp. Energy Geotech. 2023, 1–3 (2023). https://doi.org/10.59490/seg23.2023.647
13. G. Birmpilis, R. Ahmadi-Naghadeh, J. Dijkstra, Towards a methodology for the characterisation of the fabric of wet clays using X-ray scattering. In E3S Web Conf. **92**, 01005 (2019). https://doi.org/10.1051/e3sconf/20199201005
14. Y. Singh, H. Schnablegger, The SAXS guide: getting acquainted with the principles (Anton Paar GmbH, 2017).
15. M. Do Campo, B. Bauluz, F. Nieto, C. Del Papa, F. Hongn, SEM and TEM evidence of mixed-layer illite-smectite formed by dissolution-crystallization processes in continental Paleogene sequences in northwestern Argentina. Clay Miner. **51**, 723–740 (2016). https://doi.org/10.1180/claymin.2016.051.5.03
16. V. A. Drits, D. K. McCarty, The nature of diffraction effects from illite and illite-smectite consisting of interstratified trans-vacant and cis-vacant 2:1 layers; a semiquantitative technique for determination of layer-type content. Am. Mineral. **81**, 852–863 (1996). https://doi.org/10.2138/am-1996-7-807
17. T. E. Bell, Microstructure in mixed-layer illite/smectite and its relationship to the reaction of smectite to illite. Clays Clay Miner. **34**, 146–154 (1986). https://doi.org/10.1346/CCMN.1986.0340205
18. J. J. Howard, Lithium and potassium saturation of illite/smectite clays from interlaminated shales and sandstones. Clays Clay Miner. **29**, 136–142 (1981). https://doi.org/10.1346/CCMN.1981.0290208